Available online at www.sciencedirect.com
ScienceDirect
Journal of Magnetism and Magnetic Materials 306 (2006) 298–301
Journal of magnetism and magnetic materials
www.elsevier.com/locate/jmmm

# Acquisition of vector hysteresis loops from micro-arrays of nano-magnets

P.S. Keatley[a,*], V.V. Kruglyak[a], R.J. Hicken[a], J.R. Childress[b], J.A. Katine[b]

[a]School of Physics, University of Exeter, Stocker Road, Exeter EX4 4QL, UK
[b]Hitachi Global Storage Technologies, San Jose Research Center, 650 Harry Road, San Jose, CA 95120, USA

Received 10 January 2006
Available online 4 April 2006

**Abstract**

A modified scanning Kerr microscope has been used as a static Kerr magnetometer to acquire in-plane vector hysteresis loops from square Si/Ta(50 Å)/$Co_{80}Fe_{20}$(40 Å)/$Ni_{88}Fe_{12}$(108 Å)/Ta(100 Å) elements with size ranging from 123 nm to 10 μm. The nanoscale elements were arranged in square arrays of 4 μm size. The laser beam was focused to a sub-micron spot, while polarization changes were recorded with an optical bridge detector containing a beam-splitting polarizer and two quadrant photodiodes. The coercive field exhibited a non-monotonic increase from 11 Oe in the 10 μm element to 170 Oe in the 123 nm elements. Loops acquired with the field applied parallel to the easy and hard in-plane uniaxial anisotropy axes were observed to become more similar in shape as the element size decreased.


*PACS:* 75.60.–d; 75.75.+a; 75.60.Jk; 78.20.Ls

*Keywords:* Hysteresis loops; Nano-magnets; Patterned arrays; Focused MOKE

Nanoscale ferromagnetic elements are required to achieve increased storage densities within magnetic data storage technologies [1]. Magnetometry measurements provide the most direct means by which to quantify their magnetic parameters and investigate their micromagnetic state. Indeed knowledge of the magnetic ground state is a prerequisite for understanding the spin wave spectrum [2] and hence dynamic properties such as precessional switching [3] that may lead to higher data rates. Magnetometry studies of nanoscale elements have been performed with a superconducting quantum interference device [4] and an alternating gradient magnetometer [5]. However, arrays of size ~1 $cm^2$, consisting of ~$10^6$ elements of length ~100 nm and film thickness ~50 nm, were required to produce adequate signal. The magneto-optical Kerr effect (MOKE) [6] has been used to investigate the effect of configurational anisotropy [7,8], inter-element separation [9,10] and exchange bias effects within arrays of nanoscale elements [11] that are typically tens of microns in size. However, isolated microscale samples fabricated by e-beam lithography and samples integrated with microscale waveguides require a microscale probe. In this work we demonstrate static, focused Kerr magnetometry measurements that allow hysteresis loops for both components of magnetization within the sample plane to be measured simultaneously. We have performed measurements upon micro-arrays of nano-magnets, which require high sensitivity, due to the low areal density of the nano-magnets within the arrays. Excellent mechanical stability is also necessary so that the spot remains focused at the center of the array as the magnetic field is ramped up and down.

In this study measurements have been made using a scanning Kerr microscope [12] of sub-micron spatial resolution that is equipped with a compact optical quadrant bridge polarimeter. While quadrant optical bridge detectors have been used previously to image domain structures [12] and study precessional switching within microscale elements [3], measurements of in-plane vector hysteresis loops were not routinely reported.

Measurements were made upon single microscale elements and arrays of nanoscale elements. The arrays were

*Corresponding author. Tel.: +44 1392 264152; fax: +44 1392 264111.
*E-mail address:* p.s.keatley@exeter.ac.uk (P.S. Keatley).

0304-8853/$ - see front matter © 2006 Elsevier B.V. All rights reserved.
doi:10.1016/j.jmmm.2006.03.030

square, with length ~4 μm, and consisted of square elements of length(separation) 124(30), 234(77), 428(17) and 637(25) nm, while the single square elements had lengths of 2, 4, 6 and 10 μm. The elements were formed from a Ta(50 Å)/$Co_{80}Fe_{20}$(40 Å)/$Ni_{88}Fe_{12}$(108 Å)/Ta(100 Å) film sputtered onto a Si wafer and patterned by electron beam lithography and ion milling. A uniaxial anisotropy was induced in the sheet material by field annealing prior to fabrication of the elements.

MOKE measurements were performed with a mode-locked Ti:sapphire laser of 785 nm wavelength attenuated to an average power of about 10 mW. The plane polarized laser beam was expanded by a factor of ten to reduce the beam divergence and focused to a diffraction limited spot diameter ~0.8 μm with a microscope objective of numerical aperture 0.65 as shown in Fig. 1a. The measured Kerr signal yields the average response of the material within the area of the spot. An electromagnet was used to apply an in-plane magnetic field while a scanning translation stage was used to center the sample array beneath the focused laser spot. The reflected beam was collected and re-collimated by the microscope objective, and sampled using a non-polarizing beam-splitting cube. The Kerr rotation resulting from two in-plane components of the sample magnetization was measured with a vector bridge containing a Glan–Thompson polarizing beam-splitter and two quadrant photodiode detectors.

The polarizing beam-splitter is initially oriented so as to output beams of equal intensity. The Kerr rotation induced by the sample generally leads to a difference in intensity of the two beams that may be measured using the photodiodes. However in the present geometry the Kerr rotation varies across the area of the beam. The cone of rays focused onto the sample was therefore divided into four parts, enabling the longitudinal Kerr rotation from two in-plane components of the magnetization, parallel ($M_{||}$) and perpendicular ($M_{\perp}$) to the applied magnetic field $H$, to be measured as shown in Fig. 1b. For a particular magnetization component, the Kerr rotations induced on two particular halves of the reflected beam must be separately sampled and combined since they are opposite in sign and cancel if the full beam is sampled. Segmented detectors are required to isolate the signals from the different halves of the beam. By taking appropriate sums and differences of the signal outputs from the two quadrant photodiode detectors, the longitudinal Kerr rotation associated with $M_{||}$ and $M_{\perp}$ may be recovered. In order to sense $M_{||}$ beam halves $(a+d)\rightarrow(b+c)$ and $(b+c)\rightarrow(a+d)$ are used, while $M_{\perp}$ is sensed using beam halves $(a+b)\rightarrow(c+d)$ and $(c+d)\rightarrow(a+b)$, as shown in Fig. 1b.

In order to demonstrate the vector capability of the bridge, hysteresis loops acquired from the continuous reference film (coupon) are shown in Fig. 2. The magnetic field was applied parallel to the hard axis for which the sample magnetization exhibits a coherent rotation. The $M_{||}$ loop (Fig. 2a), sensed with the halves of the beam $(a+b)\rightarrow(c+d)$ and $(c+d)\rightarrow(a+b)$, and the $M_{\perp}$ loop (Fig. 2b),

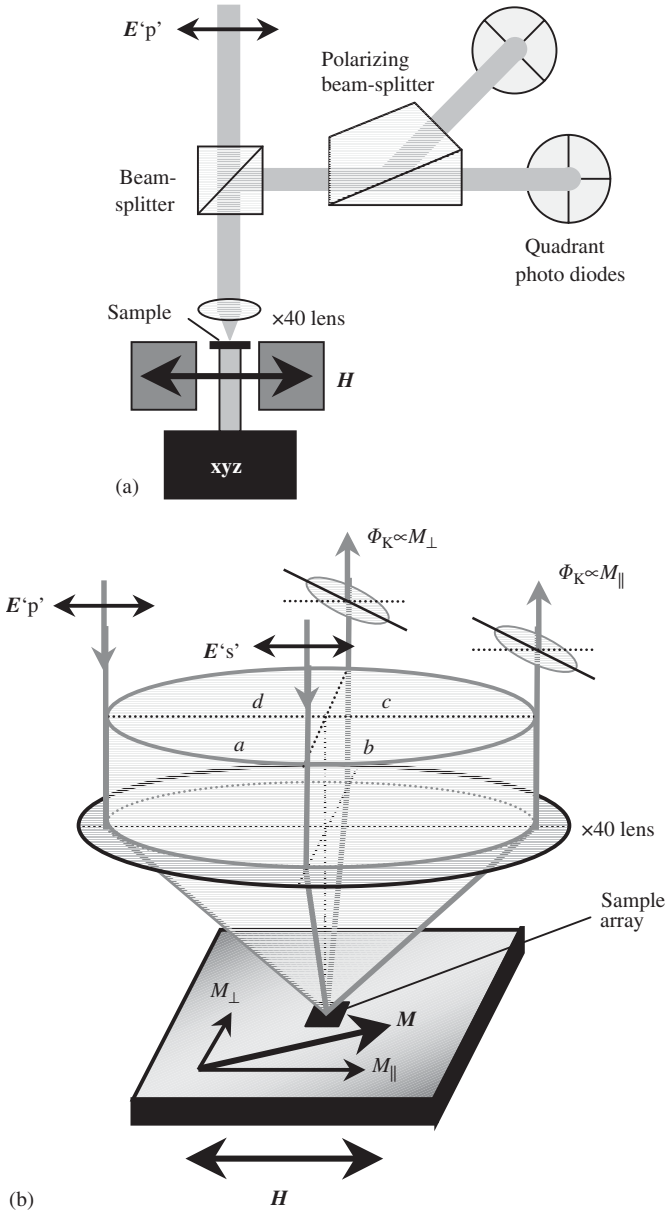


Fig. 1. (a) Schematic of the scanning Kerr microscope and optical quadrant bridge polarimeter. (b) Schematic of the laser focused upon the sample.

sensed with the halves of the beam $(a+d)\rightarrow(b+c)$ and $(b+c)\rightarrow(a+d)$, have the form predicted by the Stoner–Wohlfarth model [13]. When the sample and applied field are rotated through 90°, $M_{||}$ is instead sensed by $(a+d)\rightarrow(b+c)$, while $M_{\perp}$ is sensed by $(a+b)\rightarrow(c+d)$. Figs. 2c and d show that the hysteresis loops obtained with the orthogonal halves of the beam are now swapped over, conclusively demonstrating that the bridge measures the vector magnetization. The $M_{||}$ loops were also found to be in good agreement with those obtained from inductive looper measurements made upon a 1″ diameter reference coupon.

Fig. 3 shows $M_{||}$ and $M_{\perp}$ hysteresis loops acquired simultaneously from the 10 μm single element with the

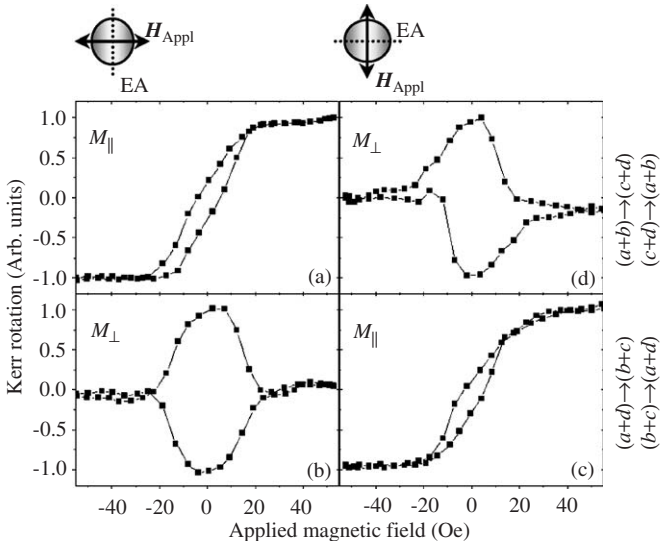


Fig. 2. Hard axis $M_{||}$ (a) and $M_{\perp}$ (b) hysteresis loops are shown for sheet material. $M_{||}$ (c) and $M_{\perp}$ (d) sensed by orthogonal halves of the focused laser beam when the sample and $\boldsymbol{H}$ are rotated through 90°.

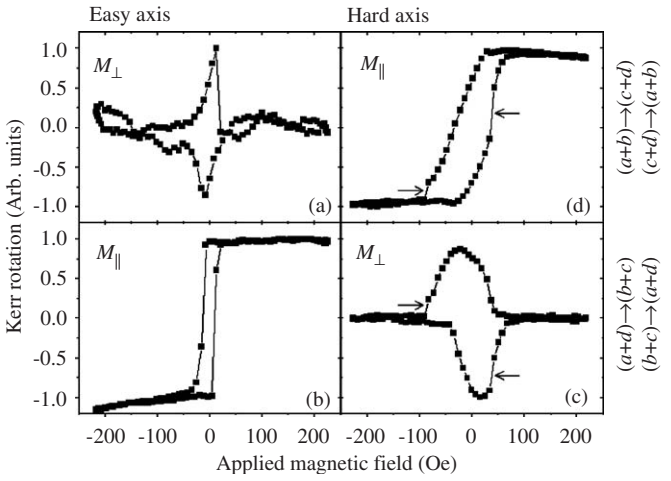


Fig. 3. Easy and hard axis $M_{||}$ and $M_{\perp}$ hysteresis loops are shown for a 10 μm single square element.

magnetic field applied parallel to the easy and hard axis directions. The easy axis $M_{||}$ loop is sensed by the half $(a+d)\rightarrow(b+c)$ and has square shape (Fig. 3b). The $M_{\perp}$ loops sensed by the half $(a+d)\rightarrow(b+c)$ reveal spikes that are correlated with the switching field in the $M_{||}$ loop (Fig. 3a). When the field is applied parallel to the hard axis, hysteresis loops with shape similar to those in Figs. 2c and d are obtained. However the hard axis loops for the 10 μm element have larger saturation and coercive field. This may be attributed to dipolar fields and pinning sites associated with the edges of the element. Discrete jumps (indicated by arrows) are well correlated between the $M_{||}$ and $M_{\perp}$ loops and suggest the occurrence of domain wall motion.

Fig. 4 shows easy and hard axis $M_{||}$ hysteresis loops acquired from the single elements and element arrays.

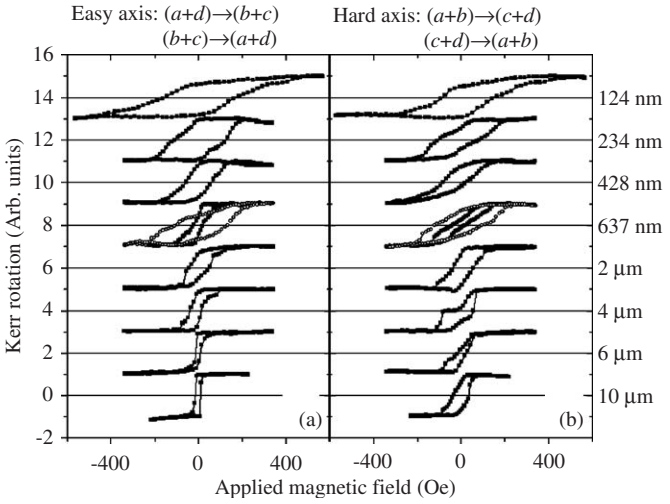


Fig. 4. $M_{||}$ easy (a) and hard (b) axis loops for all elements.

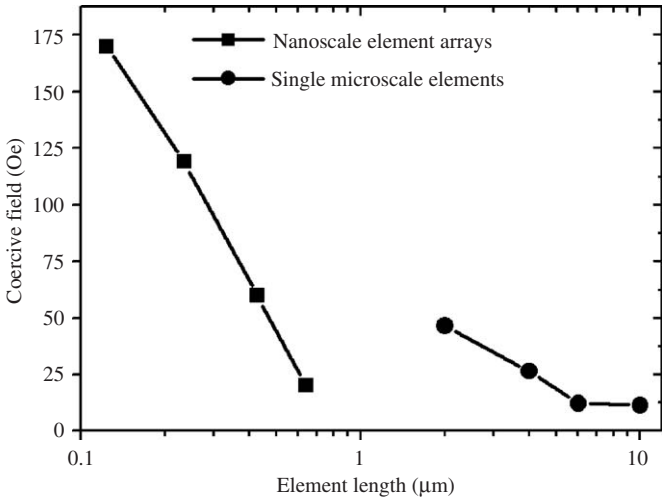


Fig. 5. Evolution of the measured coercive field of easy axis $M_{||}$ loops as the element size is reduced.

Measurable $M_{\perp}$ signals were obtained from the three largest single elements only (shown only for the 10 μm element in Figs. 3a and c). The loops in Fig. 4 were obtained in the same manner as the $M_{||}$ loops of the 10 μm element. The loops shown in Fig. 4a reveal a non-monotonic increase in coercive field from 11 Oe in the 10 μm single element to 170 Oe in the 123 nm element array. A change from a higher coercive field in the 2 μm single element to a lower coercive field in the 637 nm element array is observed, as shown for the easy axis loops in Fig. 5. A similar change is observed for the hard axis loops (Fig. 4b). One striking feature of the loops obtained from the nanoscale elements in arrays is that the shapes of the easy and hard axis loops are very similar, while for the single elements there remain significant differences between the loop shapes. For example, the easy and hard axis remanent magnetization for the 10 μm element is ~100% and ~60%, respectively, while the remanence for the

124 nm element is ~60% for both anisotropy axes. Furthermore, asymmetric switching events are seen for the hard axis loops obtained from the three largest elements, while the five smallest elements exhibit a symmetric hysteresis loop shape. In addition the loops obtained for the easy axis are symmetric for all elements measured, further demonstrating a greater similarity between easy and hard axis loops shape for the smaller elements than for the larger elements. The sudden reduction in coercive field between 2 μm and 637 nm, and the similarity of the easy and hard axis loop shapes for the nanoscale elements in arrays, may indicate a transition from domain wall motion to incoherent rotation.

There are many factors that may affect the hysteresis loop shape. Inter-element dipolar interactions within arrays may significantly modify the hysteresis loop shape with respect to the single element, e.g. by reducing the coercive field. Loops for 637 nm elements with an edge-to-edge separation of 234 nm are also shown in Fig. 4a (open circles) and show that the coercive field increases with increased element separation. We ascribe the similarity of easy and hard axis hysteresis loops shape to the increased non-uniformity of the magnetization reversal process in the four smallest elements. This is in contrast to the coherent rotation mechanism observed in the hysteresis loops of the continuous film and largest elements. The non-uniform reversal process occurs when the dipolar energy becomes more significant than the exchange energy. The difference between the easy and hard axis behavior is reduced further due to pinning at edge defects that occurs irrespective of the applied field direction. The latter effect is again more significant in the smallest elements. The random occurrence of defects leads to slanting of the hysteresis loops as the element length is decreased due to the distribution of switching fields present in the ensemble of elements. Further measurements are required to isolate the effects of these different mechanisms.

In summary, vector magnetic hysteresis loops have been obtained from continuous sheet material, individual microscale square elements and 4 μm arrays of nanoscale square elements using a scanning Kerr microscope of sub-micron spatial resolution. Measurements on sheet material have demonstrated that the vector magnetization may be sensed. Comparison of hysteresis loops obtained from different element sizes have revealed an increase in the coercive field as the element size is reduced, which has been discussed in terms of the modified dipolar fields and additional pinning sites within the elements. This work demonstrates that a scanning Kerr microscope equipped with a quadrant polarization bridge detector is a powerful tool for the characterization of nano-magnet arrays of very small area.

The authors gratefully acknowledge the support of the UK Engineering and Physical Sciences Research Council (EPSRC) and the New Energy and Industrial Technology Development Organisation (NEDO).

## References

[1] A. Moser, K. Takano, D.T. Margulies, M. Albrecht, Y. Sonobe, Y. Ikeda, S. Sun, E.E. Fullerton, J. Phys. D: Appl. Phys. 35 (2002) R157.
[2] V.V. Kruglyak, A. Barman, R.J. Hicken, J.R. Childress, J.A. Katine, Phys. Rev. B 71 (2005) 220409(R).
[3] W.K. Hiebert, G.E. Ballentine, M.R. Freeman, Phys. Rev. B 65 (2002) 140404(R).
[4] J.F. Smyth, S. Schultz, D. Kern, H. Schmid, D. Yee, J. Appl. Phys. 63 (1988) 4237.
[5] J.F. Smyth, S. Schultz, D.R. Fredkin, D.P. Kern, S.A. Rishton, H. Schmid, M. Cali, T.R. Koehler, J. Appl. Phys. 69 (1991) 5262.
[6] S.D. Bader, J.L. Erskine, in: J.A.C. Bland, B. Heinrich (Eds.), Ultrathin Magnetic Structures II, Springer, Berlin,Heidelberg, 1994 (Chapter 4).
[7] M.E. Schabes, H.N. Bertram, J. Appl. Phys. 64 (1988) 1347.
[8] R.P. Cowburn, A.O. Adeyeye, M.E. Welland, Phys. Rev. Lett. 81 (1998) 5414.
[9] C. Mathieu, C. Hartmann, M. Bauer, O. Buettner, S. Riedling, B. Roos, S.O. Demokritov, B. Hillebrands, B. Bartenlian, C. Chappert, D. Decanini, F. Rousseaux, E. Cambril, A. Müller, B. Hoffmann, U. Hartmann, Appl. Phys. Lett. 70 (1997) 2912.
[10] S.M. Weekes, F.Y. Ogrin, P.S. Keatley, J. Appl. Phys. 99 (2006) 08B102.
[11] V. Baltz, J. Sort, S. Landis, B. Rodmacq, B. Dieny, Phys. Rev. Lett. 94 (2005) 117201.
[12] W.W. Clegg, N.A.E. Heyes, E.W. Hill, C.D. Wright, J. Magn. Magn. Mater. 95 (1991) 49.
[13] E.C. Stoner, E.P. Wohlfarth, Philos. Trans. R. Soc. London A 240 (1948) 597.